Effect of Circular Arc Radius on Laser Scribing Width and Depth of Al$_2$O$_3$ Ceramics: Experiment and Numerical Simulation

Kaijin Huang [*,**,***,****], Shu Wang [***], Xian Chen [**], Haisong Huang[*], Shihao Tang[*] and Feilong Du[*]

[*] *Key Laboratory of Advanced Manufacturing Technology, Ministry of Education，Guizhou University, Guiyang 550025, P.R.China*
E-mail: huangkaijin@hust.edu.cn
[**] *Zhejiang Provincial Key Laboratory of Laser Processing Robit/ Key Laboratory of Laser Precision Processing & Detection, Wenzhou University, Wenzhou 325035, P.R. China*
[***] *State Key Laboratory of Materials Processing and Die & Mould Technology, Huazhong University of Science and Technology, Wuhan 430074, P.R. China*
,[****] *Xi'an Technological University, Shaanxi Key Laboratory of Non-Traditional Machining, Xi'an 710021, P.R. China*

Laser scribing is a promising micromachining technique for the precision production of curves like circular arc geometry on hard and brittle materials such as silicon, ceramics and glasses. The accuracy and quality of laser scribing depends on the operating parameters and geometries. In this paper, the effect of circular arc radius on the groove width and depth obtained on Al$_2$O$_3$ samples was studied experimentally, using Diode Pumped Solid State Laser Scriber, and simulated using ANSYS software. The experimental and calculated results all proved that the circular arc radius had important effect on the accuracy and quality of laser scribing due to the exist of heat accumulation effect and circular arc effect. A decrease of circular arc radius caused an increase of the groove width and depth on Al$_2$O$_3$. In addition, the center angle also had important effect on the groove width and depth due to heat accumulation effect, and an increase of center angle caused an increase of the groove width and depth on Al$_2$O$_3$.

1. Introduction

Ceramic materials especially alumina have been widely used in communications [1], automotive [2], power electronics [3], aerospace [4] and medical fields [5] due to their excellent properties such as light weight, high hardness, and high wear and corrosion resistance. The high brittleness and hardness of ceramics, on the other hand, makes their use in traditional mechanical processing, such as diamond grinding, expensive and inefficient.

With the development of laser technology, laser precision machining has attracted much attention due to the advantages of non-contact, high-speed and low cost [6] of the process, as well as the ability to obtain complex shapes such as corner angle [7], circular arc [8] and curves [9]. Among these technologies, laser scribing of hard and brittle ceramic materials such as Al$_2$O$_3$ [10], SiC [11], AlN [12,13], and carbon fiber-silicon carbide matrix (C/SiC) composite [6] has been widely used in the electronics and machinery industries. Trubelja et al. [6] investigated the effects of laser power and specimen translation velocity of laser scribing on the groove width and depth on C/SiC composites. The results were compared to theoretically predicted values obtained by solving the quasi steady state heat conduction equation in three dimensions for a moving body. Iwai et al. [10] investigated the micro scribing of Al$_2$O$_3$ with a diode-pumped Nd:YLF laser. They found that the focal position, wavelength and feed rate of the laser, as well as the number of laser scans, had important effects on the groove width and depth, and the height of Al$_2$O$_3$ debris. Modest et al. [11] investigated the stress distributions during continuous wave (CW) and pulsed laser scribing of silicon carbide based on an elastic stress model. They found that the stress fields for the scribing operations were non-symmetric and shifted towards the region in front of the laser. For both CW and pulsed scribing, a region of tensile stresses formed below material's surface, near the edge of the groove, to the side and behind the laser. Takahashi et al. [12] found that when an AlN ceramic was scribed with a CO$_2$ laser, the surface resistance was degraded. Tsai et al. [14] developed a new laser machining technique for alumina shaping, based on the principles of fracture mechanics. The fracture machining technique can be applied to shape any geometry, such as rectangular and quarter-circular corners; however, to obtain the desired contour, the CW Nd:YAG laser must be used to scribe and confine the fracture region.

So far, the investigation of laser ceramics scribing has been mainly focused on the optimization of process parameters [10,15-19] and theoretical simulations of the procedure [11,13,20]. Few works have reported the effect of geometry on groove width and depth [21,22]; however, many studies have focused on the effect of the laser cutting circular arc radius on the quality of the cuts achieved on different materials, such as metal [23-27], polymer [28,29] and ceramics [30,31]. For example, Wang et al. [23] found that

with decreasing the radii of outside arc and inside arc, the kerf roughnesses are improved; when the radius R≤7 mm, the roughnesses of these two arcs are different significantly; when the radius R>7 mm, the differences of these roughnesses almost disappear. Sharma et al. studied the effects of input process parameters (arc radius, oxygen pressure, pulse width, pulse frequency and cutting speed) on the output quality characteristics such as kerf width, deviation and taper obtained on Ni-based super alloy sheet [24,26] and Al-alloy sheet [25]. The results indicated that the optimum input parameter levels suggested for cutting curved profiles are entirely different from cutting straight profiles except kerf width [26]. Li et al. [27] studied the effects of laser cutting parameters on the quality such as the kerf width, surface roughness of the incision and slag quantity of flow curve obtained on 1Cr18Ni9Ti stainless steel. Holle et al. [28] found that with the laser power density increased, the surface radii and channel floor radius of Polydimthylsiloxane (PDMS) decrease. Sheng et al. [29] studied the curved path achieved on polymethyl-methacrylate (PMMA) by laser cutting. They found that a wider kerf width and the asymmetry between inner and outer of the kerf walls obtained compared to kerf of straight-line cutting with the curvature radius decreasing. Ji et al. [30] investigated the laser close-piercing lapping technique for damage-free cutting in arbitrary path (line, curve and angle) on Al_2O_3. Brugan et al. [31] developed laser dual-beam machining of linear trajectories and semicircular path on structural ceramics. They found that at high speeds and lower power levels, the clean fractures cannot be provided for semicircular path, but the controlled fracture can be obtained in machining of linear path using the same technology.

The application of laser scribing to ceramics presents more complications compared to steel [8,32,33]. Different circular arc radii will cause different degrees of heat accumulation, affecting the groove width and depth, which, in turn, affect the geometric accuracy of laser precision scribing. Research on this topic is therefore important to determine the applicability of the process.

In this paper, the effect of circular arc radius on the groove width and depth obtained on Al_2O_3 through laser scribing was simulated using ANSYS software and verified experimentally with the Diode Pumped Solid State (DPSS) Laser Scriber.

2. Experimental

The circular arc was scribed on Al_2O_3 ceramics using RF-P50S DPSS laser produced by Ruifeng Photoelectric Technology Company Limited in Wuhan, China. Scribing radii of circular arc are R=1 mm (sample A) and R=3mm (sample B), and substrate size of Al_2O_3 is 6×6×0.46 mm^3 (L×W×H) (Fig. 1). The groove width and depth were
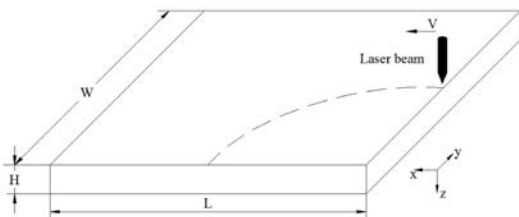
Fig. 1 Schematic diagram of laser scribing

measured with the VHX-1000 three-dimensional super depth field microscope produced by Keyence. The laser scribing parameters adopted were the following: laser power of 50 W, pulsed laser frequency of 20 kHz, laser beam radius of 0.02 mm, air pressure during blowing of 0.35 MPa, laser scribing speed of 4 mm/s, laser scanning number of 1 times.

3. Mathematical model and numerical simulation

The detailed assumptions were used to build the mathematical model can be seen in our previous paper [22]. The spatial distribution of the laser beam is in Gaussian at TEM_{00} mode.

During laser scribing, the laser beam moves on the surface of the Al_2O_3 sample with velocity V (Fig. 1). The heat transfer equation can be expressed as [34]:

$$\rho c \frac{\partial T}{\partial t} = k(\frac{\partial^2 T}{\partial x^2} + \frac{\partial^2 T}{\partial y^2} + \frac{\partial^2 T}{\partial z^2}) + Q(x, y, z, t) \quad (1)$$

where ρ is the density, c is the heat capacity, k is the thermal conductivity, and T is the temperature of the ceramic sample. Q (x, y, z, t) represents the internal heat generation rate in the body. In this paper, Q (x, y, z, t) =Q (x, y,0, t) =Q_0 is the heat source term resembling the laser beam [6].

As the laser is capable to penetrate the alumina sample, its absorption is described as Beer–Lambert bulk absorption rather than surface absorption [35]. The laser heat source, Q_0 can be treated as a heat production term and can be expressed as [6,34,36]:

$$Q_0 = \frac{2P}{\pi r^2} \cdot \frac{1}{(1-e^{-2})} \cdot a \cdot e^{-az}(1-r_f)e^{(-\frac{x^2+y^2}{r_0^2})} \quad (2)$$

where P is laser power, r is the laser beam radius, a is the absorption coefficient, r_f is the surface reflectivity [34], and r_0 is the Gaussian parameter.

The initial condition is written as:

$$T(x, y, z, 0) = T_0 = 25°C \quad (3)$$

In laser beam moving, the assisted gas flows through a coaxial nozzle towards the specimen surface. A convective flux is therefore used to define the boundary layer in correspondence of the top surface:

$$k(\frac{\partial T}{\partial x}n_x + \frac{\partial T}{\partial y}n_y + \frac{\partial T}{\partial z}n_z) = h_f(T_0 - T) \quad (4)$$

where h_f [34] is the forced convection heat transfer coefficient. With the exception of the plane of symmetry and of the bottom surface, the remaining boundary surfaces of the specimen exchange heat with the surrounding environment through natural convection. The corresponding boundary condition is expressed as:

$$k(\frac{\partial T}{\partial x}n_x + \frac{\partial T}{\partial y}n_y + \frac{\partial T}{\partial z}n_z) = h(T_0 - T) \quad (5)$$

where h is natural convection heat transfer coefficient.

The temperature distribution can be calculated by solving equations (1) – (5). The groove width and depth of laser scribing on specimen is identified as the portion of material in correspondence of which the temperature is higher than the melting temperature (2030°C) of Al_2O_3.

The laser beam moves along the surface of the Al_2O_3 ceramics plate with trajectories of different circular arc radii. A three-dimensional finite element model was devel-

oped to describe the temperature field of the sample. The results of mesh generation of samples are shown in Fig.2. To obtain the best compromise between accuracy of the result and computation time, the gradient mesh generation was used. A mesh having size of 0.01×0.01×0.046 mm^3 was used to describe the region heated by the laser, while free meshing was applied to the remaining part of the sample.
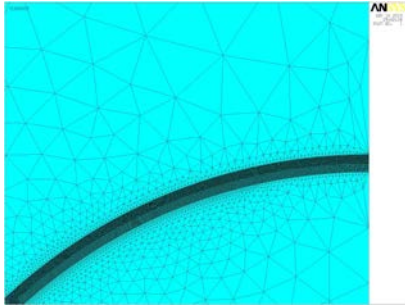
Fig. 2 Local meshing of sample: A or B

The temperature field was simulated using the finite element software ANSYS APDL command flow. An eight-node hexahedral unit was selected (SOLID 70), and the surface unit (SURF 152) was used to load the forced convection coefficient. In the thermal that followed, the simulation of specimen A required the use of 59652 hexahedral elements and 26289 nodes (Fig.3a). For specimen B, 168766 hexahedral elements and 75577 nodes were used (Fig.3b). And the computation times were about 15 and 85 h for samples A and B, respectively. The parameters used in the simulations reported in this paper are given in Table 1 [35,37–39].
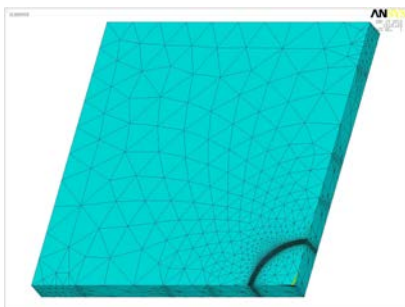
(a)
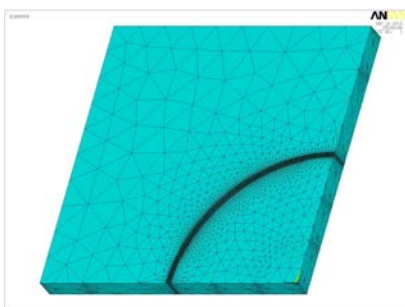
(b)

Fig. 3 Mesh generation of samples: (a) A and (b) B

Table 1 The simulated parameters

Calculating parameters	Values
Density ρ (Kg/m^3)	3720
Specific heat capacity C (J/Kg℃)	880
Thermal conductivity k (W/m℃)	25
Melting temperature T (℃)	2030
Forced convection heat transfer coefficient h$_f$ (W/m^2℃)	3000
Natural convection heat transfer coefficient h (W/m^2℃)	20
Reflectivity r$_f$	0.79
Absorption coefficient a (1/m)	6000

4. Results and discussion

Fig.4 shows the whole photographs of the whole Al$_2$O$_3$ plate after laser scribing. Fig.5 shows the picking up temperature points of different samples at different center angles θ. Fig.6 and Fig.7 are the photographs of width and the depth, respectively, of different samples in correspondence of the center angle θ=30°, after laser scribing. Both the width and depth of sample A are bigger than those of sample B. Specially, at center angle θ=30°, the measured values of groove width are 0.032 mm for sample A and 0.025 mm for sample B; the measured values of groove depth are 0.083 mm for sample A and 0.064 mm for sample B. Fig. 8 and Fig. 9 show the nephograms of temperature distribution of samples A and B, respectively, at laser scribing center angles θ of 0°, 30°, 60° and 90°.
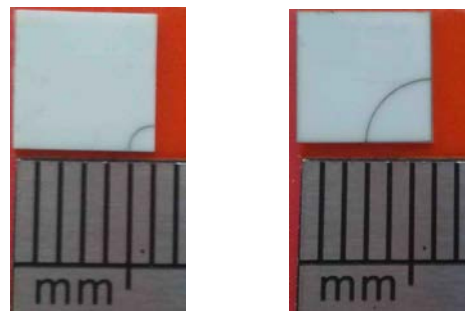
(a)   (b)

Fig. 4 Photographs of whole Al$_2$O$_3$ plates after laser scribing for samples: (a) A and (b) B
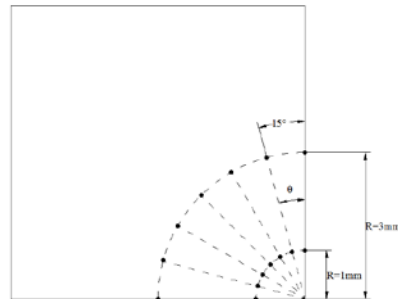
Fig. 5 Picking up temperature points of different samples at different center angles θ

First, it can be seen that with the increase of laser scribing length (corresponding to arc length Rθ in here), the calculated maximum temperatures of different samples

increase (Table 2), which shows that there is thermal accumulation effect in the process of laser scribing. Second, the calculated maximum temperature for sample A is higher than that of sample B, which shows that there is circular arc effect in the process of laser scribing.

(a)

(b)

Fig. 6 Width photographs of different samples after laser scribing at center angle θ=30° for samples (a) A and (b) B
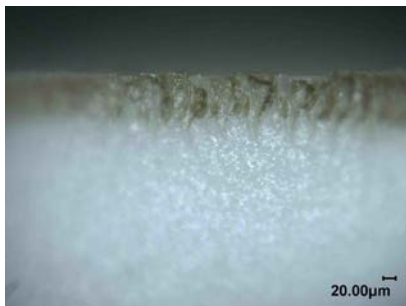
(a)
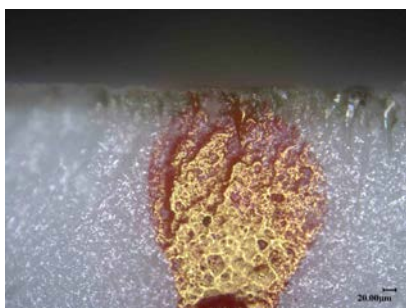
(b)

Fig. 7 Depth photographs of different samples after laser scribing at center angle θ=30° for samples (a) A and (b) B

(a) θ=0°

(b) θ=30°

(c) θ=60°
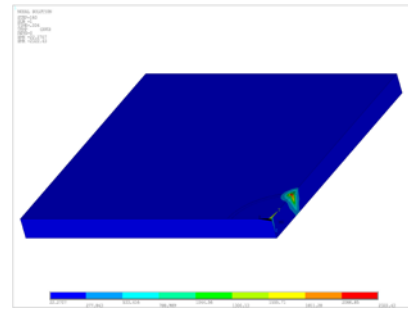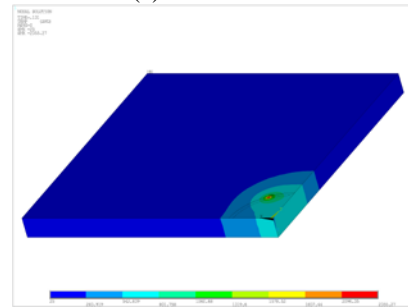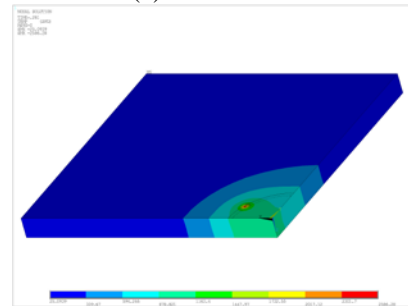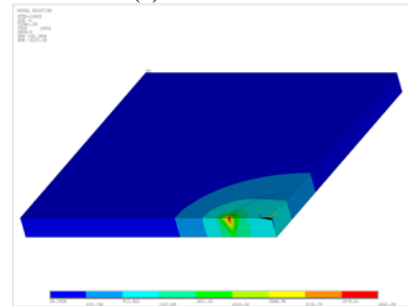
(d) θ=90°

Fig. 8 Nephograms of temperature distribution for sample A at different center angles

(a) θ=0°

13

(b) θ=30°

(c) θ=60°
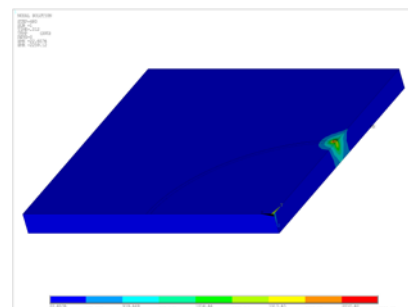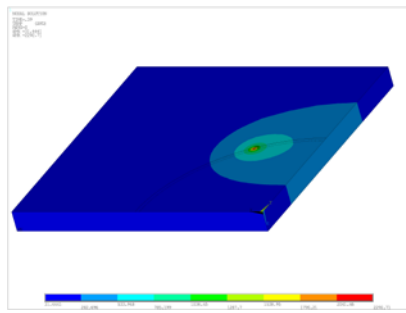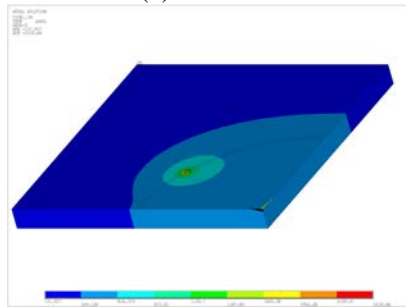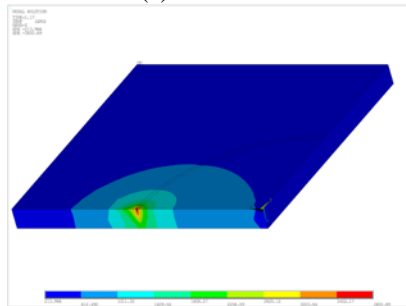
(d) θ=90°

Fig. 9 Nephograms of temperature distribution for sample B at different center angles

Table 2 Calculated temperatures at different center angles

Center angle θ	Maximum temperature of sample A (℃)	Maximum temperature of sample B (℃)
0°	2322.43	2259.12
30°	2355.27	2292.71
60°	2586.28	2416.66
90°	4020.28	3800.69

Fig. 10 and Fig. 11 are the comparisons of the groove
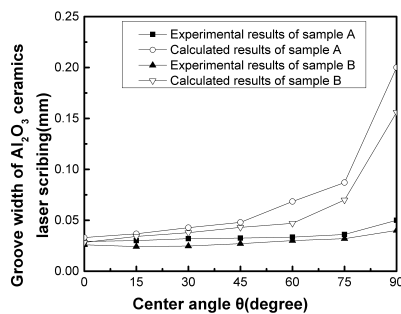
Fig. 10 Comparison between experimental results and calculated results of groove width for different samples
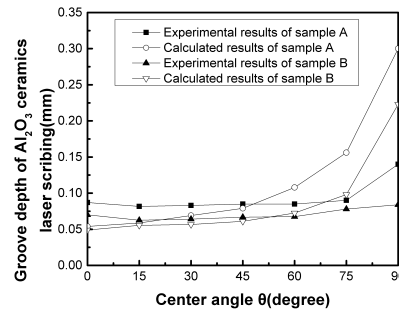
Fig. 11 Comparison between experimental results and calculated results of groove depth for different samples

width and depth for different samples based on the experimental results and the calculated results, respectively.

First, we can see that the experimental results are consistent with the trend of the calculated results. With the increase of laser scribing center angle θ, the groove width and depth for both samples increases. This is mainly due to heat accumulation effect (Table 2, Fig.12 and Fig.13). This phenomenon has been reported in laser ceramic scribing straight path [22]. Specially, the measured values of groove width increased from 0.029 mm to 0.05 mm for sample A and from 0.026 mm to 0.04mm for sample B; the measured values of groove depth increased from 0.087 mm to 0.14 mm for sample A and from 0.07 mm to 0.084 mm for sample B. Corresponding to this is that the calculated values of groove width increased from 0.033 mm to 0.2 mm for sample A and from 0.028 mm to 0.16 mm for sample B; the calculated values of groove depth increased from 0.054 mm to 0.3 mm for sample A and from 0.049 mm to 0.23 mm for sample B. It should be noted that the differences of the calculated results and the experimental results increased with the increase of laser scribing length (corresponding to arc length Rθ in here), which may be related to many factors such as mathematical model assuming, without considering the thermos-physical parameters of alumina ceramics changing with the variation of temperature, without considering thermal radiation, without considering convection heat transfer coefficient (h and h_f), reflectivity r_f and absorption coefficient α changing with temperature etc.. These will be considered in subsequent research.

Second, we can see that when the circular arc radius decreases from 3mm to 1mm, the groove width and depth of laser scribing increases. This is mainly due to circular arc effect (Table 2, Fig.12 and Fig.13). The size of the radius has important effect on heat accumulation effect of
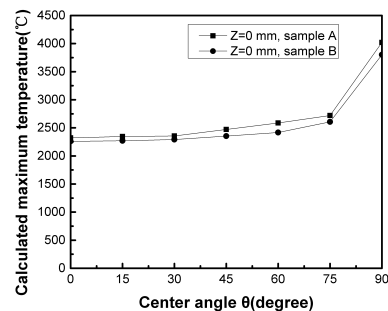
Fig. 12 Calculated maximum temperature of different samples in different positions after laser scribing 1 times
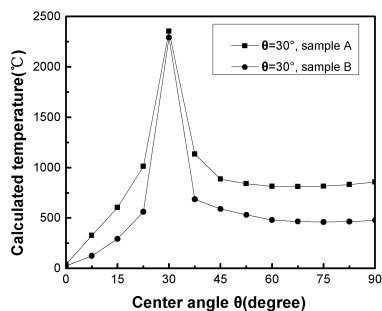
Fig. 13 Calculated temperature change of different samples at the fixed center angle θ=30° and Z=0mm after laser scribing 1 times

laser scribing. The smaller the radius, the higher the temperature (Table 2, Figs.12 and 13), resulting in the increase of groove width and depth of laser scribing (Figs. 10 and 11).

Third, for the laser scribing depth and width of different samples, both the calculated value and the experimental value all start to appear small (corresponding to center angle θ=0°~15°), then slowly increase (corresponding to center angle θ=15°~75°), and finally increase sharply (corresponding to center angle θ=75°~90°). This may be related to the heat transfer characteristics of laser scribing limited size objects.

In fact, for any laser processing technology, when a specific finite size object is heated by a laser, there are three stages in the process of laser heating, that is, the onset stage of the underheating, the intermediate stage of heat balance and the last stage of overheating. For a given radius laser scribing, the thermal heat at the three locations named the laser scribing start edge, the laser scribing middle of the part and the laser scribing end edge will increased subsequently. Specifically, in Fig.12, the calculated maximum temperatures are 2322.43℃ for sample A and 2259.12℃ for sample B at the beginning stage (corresponding to center angle θ=0° and Z=0 mm); the calculated maximum temperatures are 2346.94℃~2719.83℃ for sample A and 2262.94℃~2606.98℃ for sample B in the middle stage (corresponding to center angle θ=15°~75° and Z=0 mm); the calculated maximum temperatures of the final stage (corresponding to center angle θ=90° and Z=0 mm) are 4020.28℃ for sample A and 3800.69℃ for sample B. The start edge is less heated by laser due to lack of pre-heating (Heat dissipation is greater than heat accumulation); the laser spot ahead in the middle of the laser scribing part has been pre-heated by the laser itself during laser scribing and there the heat has been balanced (Heat dissipation is almost equal to the amount of heat accumulation); the end edge was over-heated by heat accumulation (Heat dissipation is less than heat accumulation) because there is no physical conduct to transfer the laser heat away at the end edge. So, the laser scribing depth and width are smaller at the start edge region (Figs.10 and 11, corresponding to center angle θ=0°~15°), almost constant at the laser scribing middle region (Figs.10 and 11, corresponding to center angle θ=15°~75°) and larger at the end edge region (Figs.10 and 11, corresponding to center angle θ=75°~90°).

5. Conclusions

(1) The circular arc radius has a significant effect on the groove width and depth on Al_2O_3, due to the heat accumulation effect and the circular arc effect. The effect is more evident for smaller circular arc.

(2) The center angle has a significant effect on the groove width and depth on Al_2O_3 due to the heat accumulation effect. With the increase of laser scribing center angle, the groove width and depth increases.

(3) The experimental results are consistent with the trend of the calculated results.

References
[1] F. Kouki, M. Thevenot, S. Bila, N. Delhote, T. Monediere, S. Verdeyme, and T. Chartier, Proc. 9th European Microwave Integrated Circuits Conference, Rome, (2014), p.644.
[2] N. Margaritis, L. Blum, P. Batfalsky, D. Bohmann, S. Cechini, Q. Fang, D. Federmann, J. Kroemer, Ro.Peters, and R.Steinberger-Wilckens, ECS Transactions, 68, (2015) 209.
[3] N. Akhtar, and W. Akhtar, Int. J. Energ. Res., 39, (2015) 303.
[4] A.S. Gohardani, and O. Gohardani, Aircr. Eng. Aerosp. Tec., 84, (2012) 75.
[5] F. Baino, and C. Vitale-Brovarone, Ceram Int., 41, (2015) 5213.
[6] B.S. Yilbas, S.S. Akhtar, and C. Karatas, Mach. Sci. Technol., 18, (2014) 424.
[7] B.S. Yilbas, S.S. Akhtar, and O. Keles, Int. J. Adv. Manuf. Tech., 79, (2015) 101.
[8] J. Hildenhagen, U. Engelhardt, M. Smarra, and K. Dickmann, Proc. of Frontiers in Ultrafast Optics: Biomedical, Scientific, and Industrial Applications XII, San Francisco, (2012), p.824711.
[9] M.F. Trubelja, S. Ramanathan, M.F. Modest, and V.S. Stubican, J. Am. Ceram. Soc., 77, (1994) 89.
[10] Y. Iwai, T. Mizuno, T. Arai, T. Honda, R. Tanaka, and T. Takaoka, Proc. 4th International Symposium on Laser Precision Microfabrication, Munich, (2003), p.509.
[11] M.F. Modest, and T.M. Mallision, J. Heat Trans., 123, (2001) 171.
[12] M. Takahashi, Y. Kurihara, K. Yamada, K. Kanai, and K. Kurihara, Electron. Comm. Jpn. 2., 73, (1990) 105.
[13] J.K. Lumpp, and S.D. Allen, IEEE Trans. Compon., Packag. Manuf. Technol., Part B: Adv. Packag., 20, (1997) 241.

[14] C.H. Tsai, and H.W. Chen, J. Mater. Process. Tech., 136, (2003) 166.

[15] G. David, Hybrid Circuit Technol., 8, (1991) 30.

[16] Y. Iwai, T. Arai, T. Honda, R. Tanaka, and T. Takaoka, Proc. 4th International Symposium on Laser Precision Microfabrication, Munich, (2003), p.362.

[17] M. Passler, and G. Lensch, Proc. High Power Lasers: Sources, Laser-Material Interactions, High Excitations, and Fast Dynamics in Laser Processing and Industrial Applications, (1987), p.283.

[18] M.A. Saifi, R. Borutta, Am. Ceram. Soc. Bull, 54, (1975) 986.

[19] K.G. Xia, Experimental study on laser processing of ceramic substrate[D], Shandong: Yantai University, 2009, p.41-49. (in Chinese)

[20] U.C. Paek, and V. J. Zaleckas, Am. Ceram. Soc. Bull, 54, (1975) 585.

[21] Z.G. Xu, C.S. Xu, L. Ha, and R.H. Zhou, Applied Mechanics and Materials, 217-219, (2012) 2265.

[22] K.J. Huang, S. Wang, and L. Tang, Mater. Res. Innov., 19, (2015) 239.

[23] D.W. Wang, and X.F. Gao, Chinese J. Lasers, 42, (2015) 0303005-1. (in Chinese)

[24] A. Sharma, and V. Yadava, Laser Eng., 31, (2015) 351.

[25] A. Sharma, and V. Yadava, , Opt. Laser Eng., 51, (2013) 77.

[26] A. Sharma, V. Yadava, and R. Rao, Opt. Laser Eng., 48, (2010) 915.

[27] S.Y. Li, X.G. Tian, J.D. He, and C. Liu, Chinese J. Lasers,38, (2011) 1003008-1. (in Chinese)

[28] A.W. Holle, S.H. Chao, M.R. Holl, J.M. Houkal, and D.R. Meldrum, Proc. 3rd IEEE International Conference on Automation Science and Engineering, Scottsdale, (2007), p.1119.

[29] Paul Sheng, and L.H. Cai, Int. J. Mach. Tools Manufact., 36, (1996) 739.

[30] L.F. Ji, Y.Z. Yan, Y. Bao, X.Q. Chen, and Y.J. Jiang, Chinese J. Lasers, 38, (2011) 0603002-1. (in Chinese)

[31] P. Brugan, G. Cai, R. Akarapu, and A.E. Segall, J. Laser Appl., 18, (2006) 236.

[32] C.H. Tsai, and H.W. Chen, Int. J. Adv. Manuf. Tech., 23, (2004) 342.

[33] B. Jaeggi, B. Neuenschwander, T. Meier, M. Zimmermann, and G. Hennig, Phys. Procedia, 41, (2013) 319.

[34] B.S. Yilbas, S.S. Akhtar, and C. Karatas, Int. J. Adv. Manuf. Tech., 58, (2012) 1019.

[35] Y.Z. Yan, Investigation on laser crack-free cutting of ceramics[D], Beijing University of Technology, Beijing, 2013, p.56-57. (in Chinese)

[36] W.P. Wang, B.D. Lu, and S.R. Luo, High Power Laser Part. Beams. 13, (2001) 313. (in Chinese)

[37] Y.L. Zhang, and J.P. Ma, Practical handbook of ceramic materials, (Chemical Industry Press, Beijing, 2006)p.343. (in Chinese)

[38] Blake William Clark Sedore, Laser welding of alumina ceramic substrates with two fixed beams [D], Queen's University Kingston, Canada, 2013, p.58.

[39] E. Kacar, M. Mutlu, E. Akman, A. Demir, L. Candan, T. Canel, V. Gunay, and T. Sınmazcelik, J. Mater. Process. Tech., 209, (2009) 2008.